Acid−Base Titrations of Functional Groups on the Surface of the Thermophilic Bacterium *Anoxybacillus flavithermus*: Comparing a Chemical Equilibrium Model with ATR-IR Spectroscopic Data

Hannah T. M. Heinrich,[†,‡] Phil J. Bremer,[†] Christopher J. Daughney,[§] and A. James McQuillan*[,‡]

Departments of Chemistry and Food Science, University of Otago, P.O. Box 56, Dunedin, New Zealand, and Institute of Geological and Nuclear Sciences, Lower Hutt, New Zealand

Received August 15, 2006. In Final Form: November 20, 2006

Acid−base functional groups at the surface of *Anoxybacillus flavithermus* (AF) were assigned from the modeling of batch titration data of bacterial suspensions and compared with those determined from in situ infrared spectroscopic titration analysis. The computer program FITMOD was used to generate a two-site Donnan model (site 1: pK_a = 3.26, wet concn = 2.46×10^{-4} mol g^{-1}; site 2: pK_a = 6.12, wet concn = 6.55×10^{-5} mol g^{-1}), which was able to describe data for whole exponential phase cells from both batch acid−base titrations at 0.01 M ionic strength and electrophoretic mobility measurements over a range of different pH values and ionic strengths. In agreement with information on the composition of bacterial cell walls and a considerable body of modeling literature, site 1 of the model was assigned to carboxyl groups, and site 2 was assigned to amino groups. pH difference IR spectra acquired by in situ attenuated total reflection infrared (ATR-IR) spectroscopy confirmed the presence of carboxyl groups. The spectra appear to show a carboxyl pK_a in the 3.3−4.0 range. Further peaks were assigned to phosphodiester groups, which deprotonated at slightly lower pH. The presence of amino groups could not be confirmed or discounted by IR spectroscopy, but a positively charged group corresponding to site 2 was implicated by electrophoretic mobility data. Carboxyl group speciation over a pH range of 2.3−10.3 at two different ionic strengths was further compared to modeling predictions. While model predictions were strongly influenced by the ionic strength change, pH difference IR data showed no significant change. This meant that modeling predictions agreed reasonably well with the IR data for 0.5 M ionic strength but not for 0.01 M ionic strength.

Introduction

Bacteria are unicellular organisms that have a high surface area[1] and usually an overall negative surface charge in their natural environment, making them potent binding agents for cations such as dissolved heavy metals.[2] Microbial communities are ubiquitous in near-surface fluid−rock systems,[3] and it is recognized today that they can have a significant impact upon the mobility and distribution of metal ions in the environment.[1,4] This has created an interest in the use of bacteria for the remediation of heavy-metal-contaminated wastewaters.[5] Binding of metal ions to bacteria is believed to be mediated by functional groups on the bacterial surface.[6] The cell wall of gram-positive bacteria consists of polymeric substances. The most abundant of these is peptidoglycan, which usually accounts for ca. 50% of the dry weight. Other common cell wall components are teichoic acid, teichuronic acid, and proteins.[7] Figure 1 shows model chemical structures of peptidoglycan and teichoic acid, the two main components of a typical gram-positive cell wall. Free carboxyl and amino groups located in the side chains of peptidoglycan and phosphodiester groups of teichoic acids can be protonated or deprotonated depending on the pH of the suspending medium. Teichoic acids can further contain alanyl esters with ionizable amino groups. All these groups are considered to be involved in the interactions between cell walls and metal ions.[8]

Previous attempts to quantitatively assess and predict metal binding to bacterial cell walls have used a two-step approach. First, acid−base titrations of bacterial suspensions have been conducted to identify surface functional groups. Since all titratable functional groups present contribute to the titration curve, software has been developed to calculate the pK_a's and concentrations of contributing groups based on chemical equilibrium models.[9] The obtained values have subsequently been used to model metal uptake data from batch adsorption experiments by assuming the binding of metal cations to one or two of the identified groups.[3,10,11] In several publications, it has been reported that bacterial acid−base titration curves can be modeled assuming three types of sites. On the basis of the obtained pK_a values and the known composition of cell walls, these sites are most frequently assigned as carboxyl, "phosphoryl", and amino groups.[3,10−12] It is important to be aware, however, that different sets of model parameters can provide reasonable fits to the acid−base titration data. One way to further constrain a model is to use the obtained concentration

* Corresponding author. E-mail: jmcquillan@chemistry.otago.ac.nz. Tel: +64 3 479 7928. Fax: +64 3 479 7906.

[†] Department of Food Science, University of Otago.

[‡] Department of Chemistry, University of Otago.

[§] Institute of Geological and Nuclear Sciences (GNS).

(1) Beveridge, T. J. *Annu. Rev. Microbiol.* **1989**, *43*, 147−171.

(2) van der Wal, A.; Norde, W.; Zehnder, A. J. B.; Lyklema, J. *Colloids Surf., B* **1997**, *9*, 81−100.

(3) Fein, J. B.; Daughney, C. J.; Yee, N.; Davis, T. A. *Geochim. Cosmochim. Acta* **1997**, *61*, 3319−3328.

(4) Pang, L.; Close, M. E.; Noonan, M. J.; Flintoft, M. J.; van den Brink, P. *J. Environ. Qual.* **2005**, *34*, 237−247.

(5) Schiewer, S.; Volesky, B. In *Environmental Microbe-Metal Interactions*; Lovley, D. R., Eds.; ASM Press: Washington, DC, 2000; pp 329−362.

(6) Kulczycki, E.; Ferris, F. G.; Fortin, D. *Geomicrobiol. J.* **2002**, *19*, 553−565.

(7) Hammond, S. M.; Lambert, P. A.; Rycroft, A. N. *The Bacterial Cell Surface*; Croom Helm Ltd.: Beckenham, Kent, 1984.

(8) Doyle, R. In *Metal Ions and Bacteria*; Beveridge, T. J., Doyle, R., Eds.; John Wiley & Sons: New York, 1989; pp 275−293.

(9) Westall, J. C., *FITEQL: A Computer Program for Determination of Chemical Equilibrium Constants from Expermimental Data*, version 2.0; Report 82-02; Department of Chemistry, Oregon State University: Corvallis, OR, 1982.

(10) Daughney, C. J.; Fein, J. B. *J. Colloid Interface Sci.* **1998**, *198*, 53−77.

(11) Daughney, C. J.; Fowle, D. A.; Fortin, D. E. *Geochim. Cosmochim. Acta* **2001**, *65*, 1025−1035.

(12) Wightman, P. G.; Fein, J. B.; Wesolowski, D. J.; Phelps, T. J.; Benezeth, P.; Palmer, D. A. *Geochim. Cosmochim. Acta* **2001**, *65*, 3657−3669.

10.1021/la062401j CCC: $37.00
Published on Web 01/23/2007 PAGE EST: 10

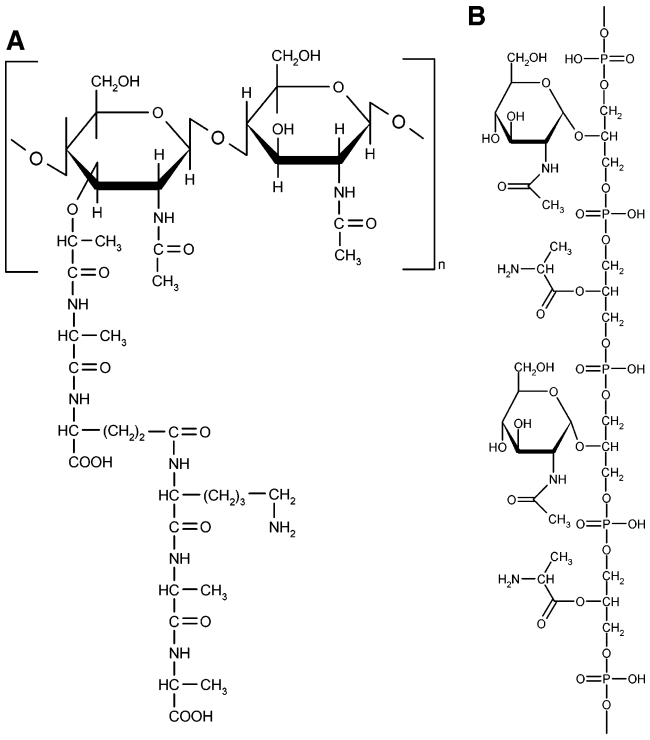

Figure 1. (A) (adapted from ref 59) Peptidoglycan monomer with commonly found amino acid composition. Glycan strands are cross-linked to varying degrees via the peptide side chains. Ionizable functional groups are free carboxyl and amino groups of amino acids. (B) An example of a simple teichoic acid. Common to all types of teichoic acids are the phosphodiester groups, which are deprotonated under physiological conditions. The arising negative charge can be modified by the presence of positively charged lysyl substituents.

and pK_a values to calculate the electrophoretic mobility of the cell at different pH and/or ionic strength values. The electrophoretic mobility is related to the overall surface charge. If the values obtained from modeling acid−base titrations are able to describe experimental electrophoretic mobility measurements; this means that the model can account for the overall bacterial surface charge, confirming the validity of the model.[13] However, to identify the chemical species present, other techniques, such as spectroscopy, are required.[3,14,15]

IR spectroscopy can be used to identify functional groups including carboxyl groups, phosphate groups, and amino groups due to their absorption bands in defined regions of the IR spectrum.[16] The technique has been used to record bacterial spectra.[17] Since the bacterial cell is comprised of a complex mixture of components, the resulting spectra show a number of composite bands. The main bands observed are generally very similar for all bacteria investigated, and assignments to functional groups have been made.[18−23] Furthermore, several studies have successfully employed the differences between IR spectra of different bacteria to discriminate between bacterial strains by statistical methods.[19,24−26]

The attenuated total reflection infrared (ATR-IR) spectroscopy technique allows bacterial cells to be monitored in situ in an aqueous environment. For this purpose, bacteria may be attached to the surface of an internal reflection element (IRE) fitted with a flow cell. Aqueous solutions of varying compositions can thus be introduced over the course of the experiment, and corresponding spectral changes can be monitored. This approach has been applied to investigate the influence of pH, ionic strength, heavy metal ions, and antimicrobial agents on bacteria.[27−29]

In the present study, we have employed both chemical equilibrium modeling of batch acid−base titrations and in situ ATR-IR pH titrations to investigate the functional groups on the surface of the thermophilic bacterium *Anoxybacillus flavithermus* (AF) in order to test the assignments of model sites to functional groups. This appears to be the first study directly correlating bacterial batch acid−base modeling with IR spectroscopic data.

First, we conducted batch acid−base titrations and electrophoretic mobility measurements of AF suspensions in sodium nitrate solutions. We were able to fit a two-site chemical equilibrium model to the data, which gave us concentrations and pK_a values of two surface groups. Second, we sought direct evidence of the functional groups on AF through the use of ATR-IR spectroscopy in NaCl solutions at different pH values and ionic strengths. Due to the multitude of components contributing to the spectrum, the distinct pH-dependent changes of carboxyl and phosphoryl groups were emphasized by using pH difference spectra. Additionally, the COOH and COO^- absorption bands of carboxyl groups were monitored to obtain direct speciation data of bacterial carboxyl groups in response to different solution pH values, which were then compared with model predictions for the speciation of site 1.

Materials and Methods

Bacterial Cultures. The thermophilic, gram-positive bacterium used in this study was an AF isolated from the drain at the Wairakei power station in Wairakei, New Zealand. Details on the isolation and cultivation of this AF have been published elsewhere.[13] Note that the previous study employed cells grown for 24 h, while the present study used cells harvested after 4 h, during the exponential phase of growth. For the IR experiments in the present study, bacteria were grown in 500 mL of tryptic soy broth (Difco) at 57 °C with constant stirring. After ca. 4 h, exponential phase cells were harvested by centrifugation (8 min, 9820 g, 20 °C). Pellets were rinsed three times by resuspension in 0.01 M $NaNO_3$ or NaCl, or 0.5 M NaCl and centrifugation (8 min, 9820 g, 4 °C). The final pellet was resuspended in the same electrolyte. NO_3^- was used because it is a bulky ion that is not easily adsorbed. NaCl was used as an electrolyte in the IR experiments to avoid complication of the spectral data by NO_3^- absorption bands.[29] Deionized (Millipore, Milli-Q) water was used to make up all washing solutions and suspending electrolytes.

Transmission Electron Microscopy (TEM). Cells were grown to the exponential phase, harvested, and washed as described above. The washing solution was 0.01 M $NaNO_3$. Washed cells were

(13) Burnett, P. G.; Heinrich, H.; Peak, D.; Bremer, P. J.; McQuillan, A. J.; Daughney, C. J. *Geochim. Cosmochim. Acta* **2006**, *70*, 1914−1927.
(14) Borrok, D.; Fein, J. B.; Kulpa, C. F. *Geochim. Cosmochim. Acta* **2004**, *68*, 3231−3238.
(15) Wightman, P. G.; Fein, J. B. *Chem. Geol.* **2005**, *216*, 177−189.
(16) Hesse, M.; Meier, H.; Zeeh, B. In *Spectroscopic Methods in Organic Chemistry*; Thieme: Stuttgart, 1997; pp 29−70.
(17) Borel, M.; Lynch, B. M. *Can. J. Appl. Spectrosc.* **1993**, *38*, 18−21.
(18) Helm, D.; Naumann, D. *FEMS Microbiol. Lett.* **1995**, *126*, 75−79.
(19) Maquelin, K.; Kirschner, C.; Choo-Smith, L. P.; van den Braak, N.; Endtz, H. P.; Naumann, D.; Puppels, G. J. *J. Microbiol. Methods* **2002**, *51*, 255−271.
(20) Feo, J. C.; Castro, M. A.; Robles, L. C.; Aller, A. J. *Anal. Bioanal. Chem.* **2004**, *378*, 1601−1607.
(21) Schmitt, J.; Flemming, H. C. *Int. Biodeterior. Biodegrad.* **1998**, *41*, 1−11.
(22) Yu, C. X.; Irudayaraj, J. *Biopolymers* **2005**, *77*, 368−377.
(23) Jiang, W.; Saxena, A.; Song, B.; Ward, B. B.; Beveridge, T. J.; Myneni, S. C. B. *Langmuir* **2004**, *20*, 11433−11442.
(24) Naumann, D.; Keller, S.; Helm, D.; Schultz, C.; Schrader, B. *J. Mol. Struct.* **1995**, *347*, 399−405.
(25) Naumann, D.; Helm, D.; Labischinski, H. *Nature* **1991**, *351*, 81−82.
(26) Lin, M.; Al-Holy, M.; Chang, S.; Huang, Y.; Cavinato, A. G.; Kang, D.; Rasco, B. A. *Int. J. Food Microbiol.* **2005**, *105*, 369−376.
(27) McWhirter, M. J.; Bremer, P. J.; McQuillan, A. J. *Langmuir* **2002**, *18*, 1904−1907.
(28) Suci, P. A.; Vrany, J. D.; Mittelman, M. W. *Biomaterials* **1998**, *19*, 327−339.
(29) Kang, S. Y.; Bremer, P. J.; Kim, K. W.; McQuillan, A. J. *Langmuir* **2006**, *22*, 286−291.

resuspended in the small volume of residual supernatant and processed in a fixative containing ruthenium red.[30] The primary fixative contained 3 mg mL^{-1} ruthenium red (ProSciTech, Australia) and 3% glutaraldehyde in 0.1 M cacodylate buffer. The secondary fixative contained 3 mg mL^{-1} ruthenium red and 2% osmium tetroxide in the same buffer. The washed pellet was embedded in agarose (Sigma-Aldrich, USA). Stepwise dehydration with ethanol and infiltration with Quetol 651 epoxy resin (ProSciTech, Australia) were performed using a Lynx el tissue processor (Australian Biomedical Corporation, Ltd., Australia). The cured blocks were cut on a Reichert−Jung Ultracut E ultramicrotome (C. Reichert AG, Austria) at a 80−90 nm section thickness and placed onto Formvar-coated slot grids. The grids were stained with uranyl acetate and lead citrate using an LKB Ultrostainer (LKB-Produkter AB, Sweden) and viewed with a Philips CM100 transmission electron microscope (Philips/FEI Corporation, Holland). Samples were positioned at the eucentric point of the specimen stage, and more than 20 longitudinal and cross-section images of the bacterial cells were recorded for measurements. The accuracy of magnification was checked by measuring a carbon cross-grating replica calibration grid (Agar Scientific, Ltd., England) under the same conditions used for the samples. Measurements agreed within 3% with the set point. Measurements were made using iTEM or analySIS Pro 3.1 software (Soft Imaging System, Germany).

Concentration Measurements of Bacterial Suspensions. The relationship between the absorbance at 600 nm (OD_{600}) and the dry biomass concentration of bacterial suspensions was determined as previously described.[13] For the determination of the relationship between wet weight and dry weight, cells were grown, harvested, and washed as described above. The washing solution was water. The final pellet was resuspended in a small volume of water, and aliquots were distributed into dry, preweighed 2 mL Eppendorf tubes and centrifuged (18300g at room temperature for 10, 15, and 25 min). The supernatant was removed after each run, and the final weight was recorded (wet weight). The tubes were dried to a constant weight at 60 °C, and the dry weights were recorded.

Batch Acid−Base Titrations. Acid−base titrations were conducted on rinsed exponential-phase cells suspended in 0.01 M $NaNO_3$ using 0.13 M HNO_3 and 0.04 M NaOH. The suspension was bubbled with nitrogen throughout the experiment to avoid interference by CO_2. The pH of the suspensions was initially adjusted to ca. 4. After a period of nitrogen purging, an up-titration to pH ∼10 was conducted followed by readjustment to pH ∼3 and a second up-titration to pH ∼10 and readjustment to pH ∼3 followed by a down-titration to pH ∼2. Six individually grown cultures were titrated, three of them in duplicate. Further details of the method have been previously published.[13]

Electrophoretic Mobility Measurements. For electrophoretic mobility measurements, cells were harvested as described above, and the pellet was split into three aliquots. The aliquots were resuspended in 0.001, 0.01, and 0.1 M $NaNO_3$, respectively, and rinsed three times in the respective electrolyte. For each electrolyte concentration, cell suspensions of different pH values were prepared in the range of pH = 2−10, and the electrophoretic mobility was measured with a Malvern Zetasizer Nano ZS (Malvern Instruments, UK). Each sample was measured twice, and the average was taken. Measurements were taken from five individually grown cultures. Details of the method have been published elsewhere.[13]

Modeling. Chemical equilibrium models were fitted to the acid−base titration data using FITMOD, a modified version of FITEQL 2.0.[9] The Donnan electrostatic model was employed. This model is a more suitable approximation for the bacterial cell wall than constant capacitance models because these were developed for "hard" inorganic particles, whereas bacteria are better represented as "soft" particles that are covered with a polyelectrolyte layer.[31] The Donnan electrostatic model assumes that the binding sites are distributed through a volume, rather than concentrated into a single plane immediately at the bacteria−water interface. For information related to the formulation of the Donnan model, see the works of Ohshima and Kondo[32] and Ohshima,[31,33] and for examples of its application in metal biosorption, see the works of Plette et al.,[34] Wasserman and Felmy,[35] Martinez et al.,[36] Yee et al.,[37] and Burnett et al.[38] Details on the modeling procedure have been published previously.[13]

IR Experiments. *Setup.* Experiments were conducted on a DigiLab FTS 4000 spectrometer (Digilab, Randolph, MA) at room temperature. The optical path was purged with dry air for 2 h prior to the experiments and throughout the experiments to avoid interference of water vapor signals. Samples were measured on a 13 internal reflection accessory 50 × 10 × 2 mm 45° ZnSe prism in a trough sampling plate (Horizon, Harrick Scientific), which will be referred to as a MIRE (multi-internal reflection element). The prism was cleaned prior to each experiment by being polished with 0.015 μm Al_2O_3 powder supported on cotton fibers and then rinsed with distilled water. For solution flow, a poly(methyl methacrylate) cover with tubing connectors was sealed to the trough with a nitrile rubber O-ring, creating a flow cell of ca. 2 mL volume. At the exit of the trough, the solution passed through a glass flow cell with fitted pH electrode (Cole Parmer, 05662) connected to a pH meter (EDT RE 357 Tx Microprocessor pH meter), allowing online monitoring of solution pH. All spectra were constructed from 64 scans at 4 cm^{-1} resolution using Digilab Win-IR Pro software.

Acid−Base Titration of Bacteria. Two milliliters of bacterial suspension (OD_{600} = 1−2 in 0.01 M NaCl solution, pH ∼5.5) were applied to the MIRE where the cells were allowed to settle onto the ZnSe surface for 90 min. After this time, the supernatant was removed with a pipet, leaving only a thin wet film of bacteria on the ZnSe surface. The cover was then attached, and 0.01 M NaCl at pH 5.5 was flowed through the cell at 1 mL min^{-1} for 90 min to remove residual suspended cells. After this washing period, the titration was conducted at the same flow rate by subsequently flowing 0.01 M NaCl solutions of different pH values through the flow-cell. Titrations were conducted from pH = 5.5 to pH = 2.3 in steps of ca. 0.5 pH units. Each solution was flowed for at least 12 min. At the end of the experiment, a solution of pH = 5.5 was flowed through the cell until a constant pH was reached (back-titration). Spectra were recorded at intervals during the process. Titrations were not fully reversible. This phenomenon may be associated with the conformational changes which are most likely responsible for the observed overall absorbance changes as discussed below. For example, compression of the polymer during the neutralization of negatively charged groups may induce chain entanglement, which may not be reversible within the time frame of the experiments. Additionally, the chemical equilibrium constants of dissociating groups may change due to their altered environment. Data from the back-titrations have not been included. Fresh cells of the same culture were used for a titration from pH = 5.5 to pH = 10.3 and back, as described for the acid titration. Titrations were conducted on four individually grown bacterial cultures. For 0.5 M ionic strength titrations, the same procedure was followed using 0.5 M NaCl solutions throughout the whole experiment. 0.5 M ionic strength titrations were conducted on two individually grown bacterial cultures. Stated pH values were obtained by averaging the maximal and minimal online pH values read during the ca. 1.5 min required to record the IR spectrum. Exemplary error bars in Figure 11 indicate the maximum and minimum pH values measured during the same period.

A principal component analysis (PCA) of the major pH-dependent spectral changes was conducted using The Unscrambler (version

(30) Handley, P. S.; Hargreaves, J.; Harty, D. W. S. *J. Gen. Microbiol.* **1988**, *134*, 3165−3172.
(31) Ohshima, H. In *Encyclopedia of Surface and Colloid Science*; Marcel Dekker, Inc.: New York, 2002; pp 1834−1852.
(32) Ohshima, H.; Kondo, T. *Biophys. Chem.* **1991**, *39*, 191−198.
(33) Ohshima, H. *Colloids Surf., A* **1995**, *103*, 249−255.
(34) Plette, A. C. C.; Vanriemsdijk, W. H.; Benedetti, M. F.; Vanderwal, A. *J. Colloid Interface Sci.* **1995**, *173*, 354−363.
(35) Wasserman, E.; Felmy, A. R. *Appl. Environ. Microbiol.* **1998**, *64*, 2295−2300.
(36) Martinez, R. E.; Smith, D. S.; Kulczycki, E.; Ferris, F. G. *J. Colloid Interface Sci.* **2002**, *253*, 130−139.
(37) Yee, N.; Fowle, D. A.; Ferris, F. G. *Geochim. Cosmochim. Acta* **2004**, *68*, 3657−3664.
(38) Burnett, P. G.; Daughney, C. J.; Peak, D. *Geochim. Cosmochim. Acta* **2006**, *70*, 5253−5269.

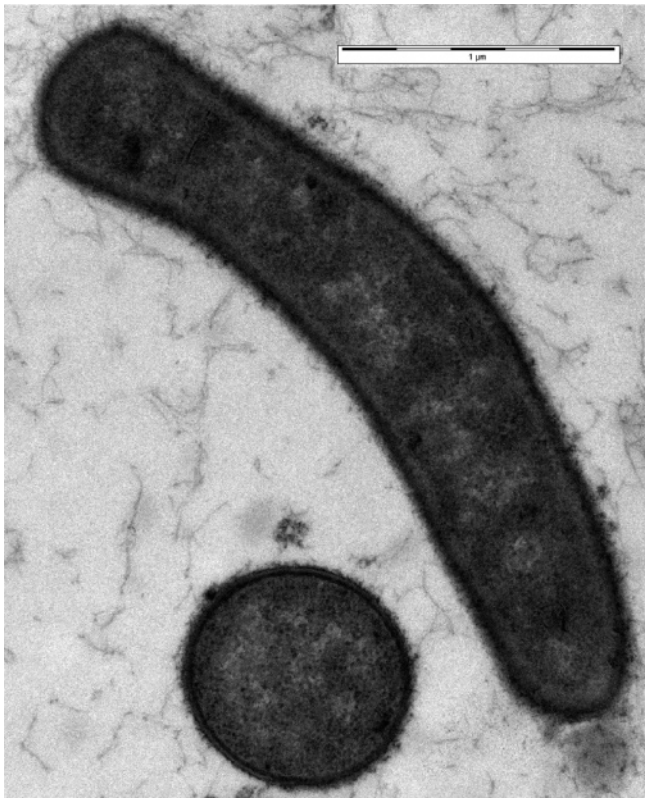

Figure 2. TEM image of ruthenium red stained thin sections (longitudinal and cross-section) of AF cells harvested during the exponential growth phase.

9.5, Camo Process As, Norway) on acid and base titration spectra (no back-titrations). The spectra were centered and scaled by the standard normal variate method and subsequently mean centered prior to PCA.

Results and Discussion

Modeling of Batch Acid−Base Titrations and Electrophoretic Mobility Measurements. The modeling procedure for acid−base titrations of bacterial suspensions has been described in detail previously.[13] Only a short description will be given here, including values for parameters that are different from those of the previous publication.

FITMOD, a modified version of FITEQL 2.0,[9] was used to describe experimental acid−base titration data on the basis of pK_a's and concentrations of bacterial surface functional groups. The approach involves proposing a set of proton active sites, e.g., two monobasic sites, one with charge 0 and one with charge +1 in their protonated forms. The corresponding protonation equilibria (e.g., eqs 1 and 2) are the basis of modeling calculations.

$$L_1 - H^0 \rightleftarrows L_1^- + H^+ \quad (1)$$

$$L_2 - H^+ \rightleftarrows L_2^0 + H^+ \quad (2)$$

In choosing a type of model, the available data on the chemistry of the investigated system are considered, and, starting with the simplest case, sets of increasing complexity are proposed until no further improvement in fit is observed. The goodness of fit is expressed in the parameter $V(Y)$, the overall variance of the error in the chemical mass balance.[39] For models involving mineral surfaces, values of $V(Y)$ between 1 and 20 indicate a reasonable fit to the data.[9] An electrostatic model is included in order to account for electrostatic interactions occurring between surface-bound functional groups depending on the electrolyte concentration. For this purpose, we considered bacteria to be soft particles according to Ohshima,[31] i.e., particles covered with a polyelectrolyte layer, with functional groups of this layer available for titration. Accordingly, we chose the Donnan model to account for electrostatic interactions because it considers the distribution of charged groups throughout a volume rather than on a flat surface.[32]

(39) Yee, N.; Fein, J. *Geochim. Cosmochim. Acta* **2001**, *65*, 2037−2042.

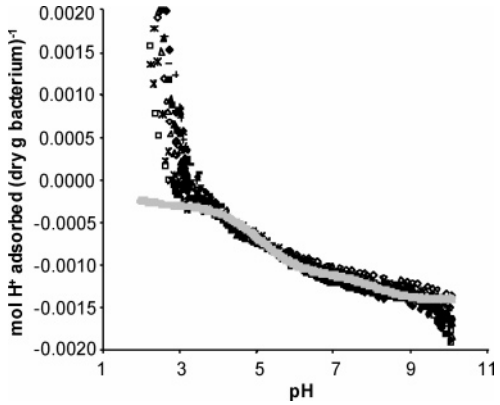

Figure 3. Batch acid−base titrations of AF from the exponential growth phase at concentrations of 0.10−0.42 dry g L^{-1} in 0.01 M $NaNO_3$. Black symbols represent data from nine titrations of six independently grown cultures, with different symbols for each titration. Grey symbols represent the respective calculated values from the best-fitting model.

Table 1. Model Parameters Generated with FITMOD for All Titrations, $V(Y) = 33.12$

	deprotonation reaction	pK_a	concentration wet (mol g^{-1})
site 1	$R-AH \rightleftharpoons R-A^- + H$	3.26	2.46×10^{-4}
site 2	$R-BH^+ \rightleftharpoons R-B + H^+$	6.12	6.55×10^{-5}

Besides the acid−base titration data, numerous parameters are required to build a model. The following approaches were used: To calculate the Donnan volume, the shape of the bacteria was approximated as a cylinder. Cell length, width, and cell wall thickness were measured from TEM images (example in Figure 2) as described above (average length, width, and cell wall thickness were 4.7 ± 1.4 μm, 0.77 ± 0.05 μm, and 36 ± 4 nm, respectively). The cell wall volume was used as the Donnan volume. The Donnan volume was thus determined to be 4.20×10^{-19} m^3 $cell^{-1}$. Absorbance measurements at 600 nm (OD_{600}) were used to estimate bacterial concentrations. Relationships between dry weight and OD_{600} and wet and dry bacterial weights were determined as dry weight (g L^{-1}) = 0.5437 × OD_{600} (R^2 = 0.98) and wet weight (g L^{-1}) = 4.561 × dry weight (g L^{-1}) (R^2 = 0.99). Using this approach, we were able to derive a chemical equilibrium model that was able to describe reasonably well the acid−base titration data from all nine titrations and the electrophoretic mobility data.

The best-fitting model had $V(Y) = 33.1$ and is summarized in Table 1. Note that, while $V(Y) < 20$ has been quoted as representing a good fit for an individual titration, the obtained $V(Y)$ value of 33.1 can be considered a good fit for a model simultaneously describing data from six individually grown cultures. Reported $V(Y)$ values for models describing data from four individual titrations range from 0.9 to 1798.[10,12] A two-site model was required to describe the data, while, for three-site models, the modeling procedure did not converge. Figure 3 shows the titration curves of six individually grown AF cultures harvested

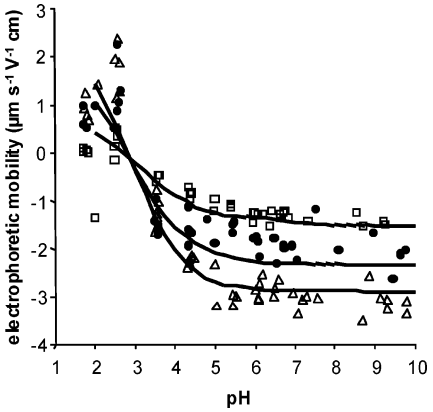

Figure 4. Electrophoretic mobility measurements of five exponential phase cultures of AF at ionic strengths 0.001 M (△), 0.01 M (●), and 0.1 M (□) and FITMOD model predictions (—).

in the exponential phase of growth. The experimental data are represented by black symbols, while the calculated values from the best-fitting model are shown in gray. The data are plotted assuming an initial proton condition[40] of zero at the observed isoelectric point of the cells. The best-fitting model does not account for further surface site protonation below pH 3, and thus the model curve does not attain positive values in Figure 3. The experimental data indicate some proton interaction with the cells below pH 3, but it is unclear whether this represents reversible proton adsorption or irreversible damage to the cell walls under acidic conditions,[41] and so the data below pH 3 have not been used to constrain the model.

Titration data reflect protonation and deprotonation reactions regardless of the charge of the dissociating groups. To further constrain the model, the obtained pK_a values and site concentrations were used to fit experimental electrophoretic mobility data at different pH and ionic strength values. The electrophoretic mobility gives estimates of the overall bacterial surface charge and of the isoelectric point. Since the overall surface charge, similar to the overall buffering capacity, which is measured in the batch acid−base titrations, represents the sum of all ionized surface groups at a given pH and ionic strength, a realistic model should be able to describe both data sets reasonably well. Calculation of the electrophoretic mobility, however, requires several parameters that could not be determined from our experimental data. Using literature-based assumptions and variation of factors over a reasonable range as outlined previously,[13] the models described here include values of 2.35×10^{-6} m, 180, and 5×10^{-10} for the effective particle radius *a*, the conductivity ratio $K^{\sigma,i}/K^{\sigma,d}$, and the ionic drag factor *m*, respectively. Figure 4 shows electrophoretic mobility measurements from five independently grown cultures at different ionic strengths (symbols) and calculated curves (lines).

It is clear from the electrophoretic mobility data, that the cell wall can acquire an overall positive or negative charge depending on pH, which suggests that both positively and negatively charged groups are present in varying concentrations. From the literature on bacterial cell wall composition, it seems most likely that, in agreement with our proposed model, two monobasic sites, namely, amino and carboxyl groups, account for the charge rather than one type of dibasic site. According to this theory, site 1 of the model represents carboxyl groups on the bacterial surface. The calculated pK_a value of the site (3.26) supports this assignment.

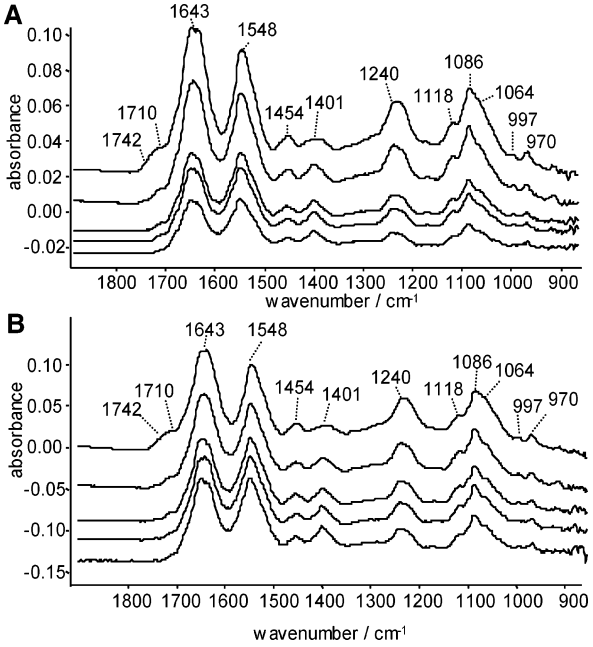

Figure 5. (A) ATR-IR spectra of AF harvested during the exponential growth phase recorded on ZnSe in 0.01 M NaCl at pH values of (bottom to top) ca. 10, 8, 6, 4, and 2.5. The spectra are offset vertically. (B) Spectra normalized to an absorbance of 0.1 at 1548 cm^{-1}.

Site 2 is most likely to represent amino groups in peptidoglycan, surface proteins or alanyl substituents on teichoic acids. While the solution pK_a for a primary amine such as propylamine is >10, pK_a values of 7−9 have been reported for amino groups in peptides or proteins,[42,43] and surface pK_a values of 4−7 have been reported for amino groups in self-assembled monolayers.[44−46] The pK_a of site 2 (6.12) falls into this latter range. Agreement between electrophoretic mobility measurements and model predictions provides further support for the validity of the proposed model.

This model for exponential-phase AF is different from most publications on chemical equilibrium models of bacterial surface groups in that it does not require the presence of a third site. Interestingly, acid−base titrations of AF in the stationary/death phase were also best described by a three-site Donnan chemical equilibrium model,[13] emphasizing the importance of culturing conditions in studies on bacteria.

ATR-IR Spectroscopy. *Peak Assignments.* During IR titrations, the overall absorbance of bacterial spectra increased with decreasing pH (Figure 5A). This phenomenon was previously observed by McWhirter et al.[27] It has been ascribed to the compression of surface polymers upon neutralization of their inherent negative charge by protons or other cations causing bacteria to settle down closer to the surface of the MIRE. This affects the absorption intensity of the whole spectrum and complicates the evaluation of relative absorbance changes of specific peaks. Changes in the amide I band are nonsystematic due to variable water and/or water vapor signal intensities. The amide II band (∼1548 cm^{-1}) of the bacterial spectrum was used as an internal standard for the total cell mass. This approach has been utilized in other studies on bacterial samples.[17,47] Ishida

(40) Fein, J. B.; Boily, J. F.; Yee, N.; Gorman-Lewis, D.; Turner, B. F. *Geochim. Cosmochim. Acta* **2005**, *69*, 1123−1132.
(41) Borrok, D.; Fein, J. B.; Tischler, M.; O'Loughlin, E.; Meyer, H.; Liss, M.; Kemner, K. M. *Chem. Geol.* **2004**, *209*, 107−119.
(42) Leach, S. J.; Lindley, H. *Aust. J. Chem.* **1954**, *7*, 71−74.
(43) Sakakiba. R; Hamaguch, K. *J. Biochem. (Tokyo)* **1968**, *64*, 613−618.
(44) Wang, B.; Oleschuk, R. D.; Horton, J. H. *Langmuir* **2005**, *21*, 1290−1298.
(45) Nishiyama, K.; Kubo, A.; Ueda, A.; Taniguchi, I. *Chem. Lett.* **2002**, 80−81.
(46) van der Vegte, E. W.; Hadziioannou, G. *J. Phys. Chem. B* **1997**, *101*, 9563−9569.

and Griffiths found for transmission spectra of aqueous protein solutions that changes in pH did not change the amide II intensity. They also showed that, in the absence of conformation changes, the relative intensities of bands in ATR-IR spectra of thin films should be equal to those obtained by transmission IR.[48] These observations support the use of the amide II band as an internal standard even under varying pH conditions. While changes in protein conformation may occur during the titration, this is usually most evident in shifts of the amide I band, as observed, for example, by Omoike and Chorover[49] for the amide I band of extracellular polymers. In the present study, however, no shift in the wavenumber of the amide I band was observed, and the amide II band is generally less sensitive to conformational changes than the amide I band.[49] It seems, therefore, that, in this case, the amide II band should provide a reasonable point of reference for the comparison of relative intensity changes.

Spectra at different pH values normalized to an absorbance of 0.1 at the amide II band are shown in Figure 5B. Amide II absorbances before normalization ranged from 0.02 to 0.09 for 0.01 M titrations and from 0.02 to 0.04 for 0.5 M titrations. Bacterial spectra at 0.5 M ionic strength looked the same as those at 0.01 M ionic strength (data not shown).

The spectra are composed of a number of broad bands that accommodate contributions from various IR absorbing groups. The most prominent bands are amide I (1643 cm^{-1}) and amide II (1548 cm^{-1}).[50,51] Different forms of phosphate and polysaccharides contribute to an array of peaks between 1150 and 950 cm^{-1}.[22,23] A broad peak around 1240 cm^{-1} has been assigned to phosphate and carboxylic acid/ester moieties and may also contain the amide III band.[19,22,23] The band at ~1454 cm^{-1} has been assigned to methyl and methylene deformation modes.[18,19,22,23,26] C−H stretching modes were observed in the spectral region at 2800−3000 cm^{-1}. A band at ~1400 cm^{-1} has been assigned to a superimposition of C−O−H in-plane bending and $C(CH_3)_2$ stretching by Yu and Irudayaraj[22] based on the fact that they found a prominent peak in this position in the cytoplasm where a high concentration of carboxylic acids is not expected. However, our spectra at different pH values show an increase in relative intensity of the 1401 cm^{-1} band with increasing pH. This indicates a contribution from carboxylate absorptions, which also agrees with the assignments by other authors.[18,19,23] The shoulder at ~1720 cm^{-1} on the amide I band, which decreases in absorbance with increasing pH, is due to the corresponding protonated carboxylic acid groups.[19,23] Carboxylic acid signals in bacteria are attributed to amino acids in peptidoglycan and proteins. Free carboxyl groups may occur as C-terminal groups or as free side-chain carboxyls of glutamic and aspartic acid. A sharp peak at 1400 cm^{-1} comparable to the one observed in bacterial difference spectra (Figure 6) has been observed for aqueous solutions of glutamate.[52] It is possible that much of the observed carboxyl signal stems from glutamic acid residues. Further pH-dependent changes observable in Figure 5B are changes in the shape and intensity of the bands around 1240 and 1086 cm^{-1}. A small peak is observed at 970 cm^{-1}. The presence of phosphomonoester groups (−O−$PO(OH)_2$) in a bacterial spectrum would be most readily discerned by a decrease in the intensity of the isolated

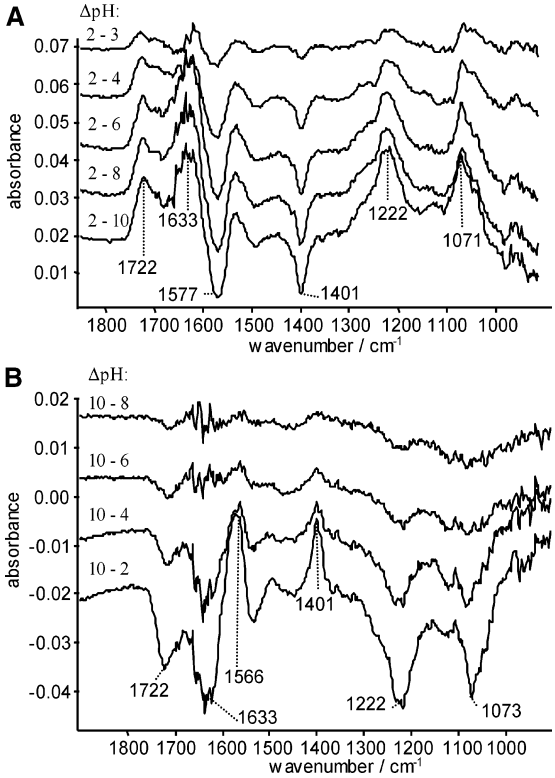

Figure 6. ATR-IR pH difference spectra of AF harvested in the exponential growth phase recorded on ZnSe in 0.01 M NaCl. The spectra are offset on absorbance scale for clarity. (A) $\Delta pH = 2 - x$: spectra at (bottom to top) pH = 10.0, 8.0, 6.0, 3.9, and 3.0 subtracted from the spectrum at pH = 2.3. (B) $\Delta pH = 10 - x$: spectra at (bottom to top) pH = 2.3, 3.9, 6.0, and 8.0 subtracted from the spectrum at pH = 10.0. (Decreased spectral quality of difference spectra when using a basic reference spectrum has been reported previously by Gershevitz et al.[57] for the titration of carboxylate-functional monolayer assemblies.)

symmetric P−O stretch of the dianion (−O−PO_3^{2-}) at ~980 cm^{-1} with monoprotonation. For example, glucose-6-phosphate with a second pK_a of 6.32 loses a symmetric P−O stretch peak at 978 cm^{-1} upon monoprotonation of its dianion.[53] While there is a small peak at 970 cm^{-1} in the Figure 5B spectra, almost all of the titrations carried out showed no absorbance decrease of the 970 cm^{-1} peak in the pH range of 7 to 5. Since the 970 cm^{-1} peak of the bacterial spectrum is very small, and systematic pH-dependent changes were not reproducibly observed, the spectral data do not appear to indicate significant concentrations of phosphomonoesters.

To isolate the pH-dependent spectral changes and allow their evaluation, difference spectra were acquired by subtracting all spectra from the spectra at the lowest and highest pH of the titration (i.e., pH ~ 2.3 and pH ~ 10.3; the subscripts $2-x$ and $10-x$ will be used to indicate the resulting spectra at pH = x). Examples of resulting spectra are shown in Figure 6. Among the prominent features are the bands due to stretching vibrations (ν) of the protonated and deprotonated forms of carboxylic acid groups ($\nu^{s}_{COO^-}$ at ~1401 cm^{-1}, $\nu^{as}_{COO^-}$ at ~1577 cm^{-1}, $\nu^{C=O}_{COOH}$ at ~1722 cm^{-1}, ν^{C-O}_{COOH} at ~1222 cm^{-1}). While the peaks at 1577 and 1222 cm^{-1} are affected by underlying water and P═O contributions, a distinct peak of pH-dependent intensity at 1401 cm^{-1} marks the deprotonated form of carboxylic acid groups. This peak was used to monitor carboxyl speciation based on IR spectra as discussed below.

(47) Naumann, D.; Schultz, C.; Helm, D. In *Infrared Spectroscopy of Biomolecules*; Mantsch, H. H., Chapman, D., Eds.; Wiley-Liss: New York, 1996; pp 279−310.
(48) Ishida, K. P.; Griffiths, P. R. *Appl. Spectrosc.* **1993**, *47*, 584−589.
(49) Omoike, A.; Chorover, J. *Biomacromolecules* **2004**, *5*, 1219−1230.
(50) Landa, A. S.; van der Mei, H. C.; Busscher, H. J. *Adv. Dent. Res.* **1997**, *11*, 528−538.
(51) McWhirter, M. J.; McQuillan, A. J.; Bremer, P. J. *Colloids Surf., B* **2002**, *26*, 365−372.
(52) Roddick-Lanzilotta, A. D.; McQuillan, A. J. *J. Colloid Interface Sci.* **2000**, *227*, 48−54.
(53) Nakanishi, K.; Hashimoto, A.; Pan, T.; Kanou, M.; Kameoka, T. *Appl. Spectrosc.* **2003**, *57*, 1510−1516.

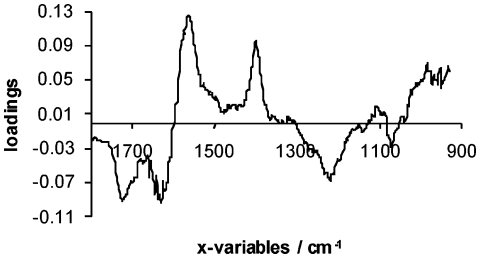

Figure 7. PCA loadings of PC1 (explained variance 77%) for the 1800−930 cm^{-1} region of acid and base titration spectra recorded in 0.01 M NaCl for one exponential phase AF culture.

In addition to the carboxylic acid bands, two more prominent bands are found in the difference spectra. Asymmetric and symmetric stretching of phosphodiester groups ($>PO_2^-$) contribute to these peaks at ∼1220 and ∼1086 cm^{-1}.[47] The absorption bands for protonated and deprotonated forms of phosphodiesters are not as well separated as the carboxyl bands. In difference spectra, intensity changes in the overlapping peaks of the protonated and deprotonated forms do not produce separated positive and negative peaks, but lead to spectral features resembling the first derivative of a peak. Such features are seen most clearly in the difference between the pH = 4 and pH = 2.3 spectra in Figure 6A near 1070 cm^{-1} and less distinctly near 1222 cm^{-1}. Changes in these regions take place with increasing pH up to pH = 4. This indicates that, above pH = 4, phosphodiesters are fully deprotonated. Since total protonation of phosphodiester groups was not achieved within the titration range, we can only state that the apparent pK_a of phosphodiester moieties of AF under the given experimental conditions is <4.

Other ionizable groups expected to be present at the bacterial surface, as seen from Figure 1, are hydroxyl and amino groups. Hydroxyl and amino groups could not be identified in either the direct or the difference spectra. Hydroxyl groups are not expected to deprotonate in the pH range investigated. The direct spectral observation of OH deformation bands is complicated by vibrational coupling and overlap with phosphate absorptions.[23] Ammonium ($-NH_3^+$) groups have a weak degenerate deformation band occurring at around 1600 cm^{-1} and a stronger symmetric deformation band that occurs in the region 1500−1550 cm^{-1}. Any deprotonation of an ammonium group would most readily be detected in an absorption loss at 1500−1550 cm^{-1}, as the most definite mode of the neutral amino groups ($-NH_2$) occurs in the region 1590−1650 cm^{-1}, overlapping with the region of the $-NH_3^+$ deformation.[54] All these bands are relatively weak and could not be detected in the direct spectra. Moreover, the 1500−1550 cm^{-1} region of the bacterial spectra is also affected by changes in the antisymmetric carboxylate stretch and the water OH bending mode absorption, resulting in no significant evidence of ammonium deprotonation in either the direct or the difference spectra.

A PCA of the data confirmed the findings of the difference spectra. The loadings plot for principal component 1 (PC1), which accounted for 77% of the total variance, is shown in Figure 7. The loadings indicate that most spectral variation during the pH titration is due to changes in the carboxyl regions. The possible contributions of carboxyl and phosphodiester groups in the 1200 cm^{-1} region cannot be further distinguished; however, the phosphodiester region near 1080 cm^{-1} shows the change of two peaks in opposite directions, which appears as a derivative type shape in the difference spectra.

In summary, the IR data in the pH range from 2 to 10 showed peaks related to amide, carboxyl, and phosphodiester moieties; however, no bands related to hydroxyl or amino groups, which are also expected to be present on the bacterial cell surface, could be identified. Phosphomonoester groups could not unequivocally be detected. The intensity of the amide II band served as an internal standard. Changes in the protonation state of phosphodiesters were observed in the pH region of 2−4, and changes in the protonation state of carboxyl groups were observed in the pH region of 2−7. While the pK_a of phosphodiester groups could only be narrowed down to a value below 4, we have attempted to obtain quantitative information on carboxyl speciation as detailed below.

Carboxyl Speciation Changes with pH. A general account of the procedures illustrated by 0.01 M ionic strength data will be given first, followed by a short discussion of 0.5 M ionic strength data.

The quantitative assessment of carboxyl speciation is complicated by several factors: First the overall absorbance change in the bacterial spectrum with pH indicates that a varying concentration of bacteria, and therefore a varying number of carboxyl groups, is sampled by the IR beam at different pH values. The total number of carboxyl groups contributing to the measured absorbance is not known, but, after normalization to the amide II band, it is assumed to be constant:

$$c_{tot} = c_{COO^-,\,x} + c_{COOH,\,x} \quad (3)$$

where c_{tot} represents the total concentration of carboxyl groups, and $c_{COO^-,\,x}$ and $c_{COOH,\,x}$ are the concentrations of the deprotonated and protonated carboxyl groups at pH = x, respectively.

The concentration of carboxylates is related to their absorbance at a given wavenumber via the Beer−Lambert law [There is a possibility that bacterial suspensions do not fulfill all the prerequisites of the Beer−Lambert law.[60] The condition of infinite dilution is presumably strictly fulfilled neither in terms of absorbance of carboxyl groups nor in terms of light scattering by the cells in the evanescent wave. The simultaneous occurrence of absorption and scattering in the sample as well as the varying bacterial concentration near the prism in response to protonation/deprotonation and the resulting different probabilities of shadowing all add to the complexity of the situation. Practically speaking, however, the Beer−Lambert law is the basis for diverse quantitative applications of spectroscopy,[61] and the relationship between the OD_{600} and concentration of our samples showed a linear relationship (R^2 = 0.98)]:

$$A_{COO^-,\,x} = \epsilon_{COO^-} \times c_{COO^-,\,x} \times l \quad (4)$$

where A is the absorbance, ϵ is the molar absorption coefficient, and l is the path length of the sample. Since all absorbances were measured on the same prism on the same sample, the path length (an effective path length for internal reflection[55]) is assumed to be constant.

Furthermore, since the carboxyl bands are part of complex bacterial absorbance patterns, bacterial carboxyl absorbances had to be obtained from pH difference spectra. The resulting absorbances (ΔA) will be indicated by subscripts $2-x$ and $10-x$, respectively, where $2-x$ refers to the spectrum at pH = x subtracted from the spectrum at pH ∼ 2.3 (lowest pH of titration). The resulting absorbances at pH = x therefore correspond to the relative protonation ($10-x$) and deprotonation ($2-x$) of carboxyl

(54) Pearson, J. F.; Slifkin, M. A. *Spectrochim. Acta, Part A* **1972**, *28*, 2403−2417.

(55) Harrick, N. S. *Internal Reflection Spectroscopy*; Harrick Scientific Corporation: New York, 1966.

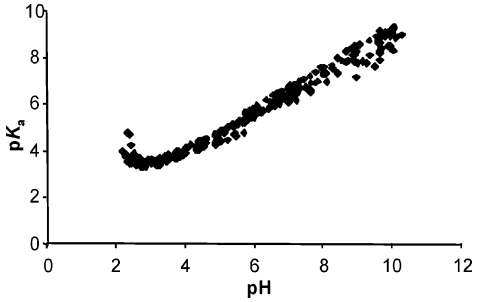

Figure 8. Calculated carboxyl group pK_a values from the Henderson−Hasselbalch equation for four exponential phase cultures of AF titrated at 0.01 M ionic strength plotted against pH.

groups compared to the pH extremes. If it is assumed that carboxyl groups are completely deprotonated at the highest pH of the titration and completely protonated at the lowest pH, the combination of eqs 3 and 4 with l and ϵ being constant gives the following expression for the concentration ratio of protonated to deprotonated carboxyl groups at pH = x:

$$\frac{c_{\mathrm{COOH},\,x}}{c_{\mathrm{COO^-},\,x}} = -\frac{\Delta A_{\mathrm{COO^-},10-x}}{\Delta A_{\mathrm{COO^-},2-x}} \tag{5}$$

The equilibrium constant for the dissociation of a monocarboxylic acid (RCOOH) at a bacterial surface,

$$\mathrm{RCOOH} \rightleftarrows \mathrm{RCOO^-} + \mathrm{H^+}$$

is

$$K = \frac{c_{\mathrm{RCOO^-}} \times a_{\mathrm{H^+}}}{c_{\mathrm{RCOOH}}} \tag{6}$$

where a_{H^+} indicates the proton activity.[13] The logarithmic form of this expression is known as the Henderson−Hasselbalch equation and can be used to calculate the pK_a of the dissociating group:

$$\mathrm{p}K_a = \mathrm{pH} + \lg \frac{c_{\mathrm{COOH}}}{c_{\mathrm{COO^-}}} \tag{7}$$

The values for pK_a calculated from the IR data over the titration range are plotted against pH in Figure 8. The graph shows a wide range of pK_a values. While this deviation from ideal behavior (horizontal line indicating one distinct pK_a) might be due to the many complex interactions that can occur on the bacterial surface, one practical aspect of determining the concentration ratio via the absorbance ratio is that, since concentration changes and therefore absorbance changes decrease exponentially on either side of the pK_a value, absorbance changes are most reliably determined within 1 pH unit on either side of the pK_a value of the investigated group. It is therefore instructive to plot the pK_a values, not over pH, but over the concentration ratio of deprotonated to total carboxyl groups. The carboxylate ratio is calculated from the carboxylate absorbance:

$$\frac{c_{\mathrm{COO^-}}}{c_{\mathrm{tot}}} = \frac{\Delta A_{\mathrm{COO^-},2-x}}{\Delta A_{\mathrm{COO^-},2-10}} \tag{8}$$

The resulting graph (Figure 9A) shows a largely horizontal line up to a carboxylate ratio of ca. 0.6, after which the pK_a as well as the scattering of the data greatly increases. From the horizontal part of the graph, a pK_a of 3.3−4.0 can be estimated.

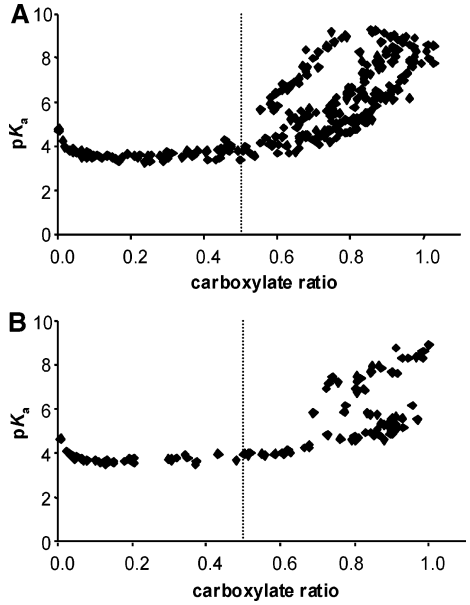

Figure 9. Calculated carboxyl group pK_a values from the Henderson−Hasselbalch equation for exponential phase cultures of AF plotted against the carboxylate ratio; the vertical line indicates half protonation: (A) 0.01 M ionic strength (four cultures); (B) 0.5 M ionic strength (two cultures).

In contrast to modeling results, the IR data allow the identification of carboxyl groups. However, the nonideal graphs resulting from the above calculations confirm that bacterial carboxyl groups cannot simply be treated as free carboxyl groups in dilute solutions (applicability of Henderson−Hasselbalch), and pK_a values derived from the Henderson−Hasselbalch equation are not a strong basis for testing the calculated model pK_a. However, the IR data do provide direct evidence of the carboxyl speciation. Comparison of the ratio of the protonated to deprotonated carboxyl concentrations derived from the IR data via eq 5 and calculated for site 1 of the model (0.01 M ionic strength) plotted over the pH range (Figure 10A) did not show good agreement between the curves.

In evaluating the misfit between model and data, we need to consider improvements that may be made in the IR data analysis as well as in the model. Both data and model are for the carboxyl groups on the intact bacterium at an ionic strength of 0.01 M. The two modifications made to the IR data are normalization and subtraction. Given the overall absorbance changes of the bacterial spectrum, normalization to an internal standard is a necessary requirement for making any quantitative estimations based on absorbance measurements. While there is the possibility that the amide II band is slightly affected by pH changes (e.g., varying degrees of hydrogen bonding), no other bacterial band seems to be better suited as an internal standard, and it has been used by other investigators for this purpose.[17,47]

In using absorbance changes from difference spectra it was assumed that the reference spectra represented states of full protonation and deprotonation respectively. While the assumption of full deprotonation at pH = 10 seems justified for a carboxyl group, full protonation may not occur at pH = 2.3. Plotting the COOH and COO^- absorbances over pH (Figure 11) shows that absorbance values level out at pH > 7, justifying the assumption of full deprotonation at pH = 10. In the low pH region, no plateau is reached within the titration range, suggesting that full protonation is not achieved. Practically, the titration range at the acidic end is limited by the onset of decomposition of the MIRE (ZnSe releases H_2Se and Zn^{2+} at low pH) and the bacteria (no spectral evidence of cell disruption was observed; however,

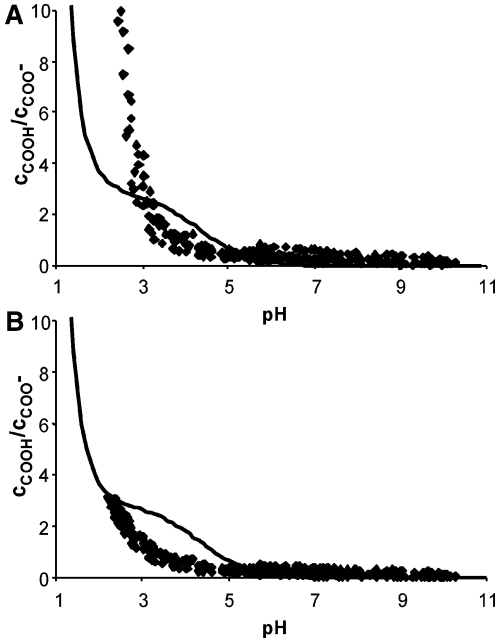

Figure 10. Carboxyl speciation for four exponential phase cultures of AF titrated at 0.01 M ionic strength plotted against pH; symbols indicate IR data, and the line represents speciation output for site 1 of the model. (A) IR data for full protonation of carboxyl groups at the lowest pH of the titration (∼2.3). (B) IR data corrected for incomplete protonation at the lowest pH of the titration according to the model.

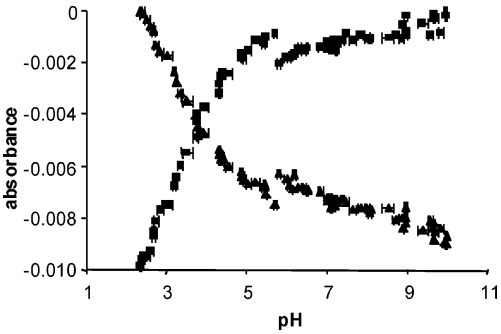

Figure 11. Absorbances of (■) COOH (1722 cm^{-1}, $10 - x$) and (▲) COO^- (1401 cm^{-1}, $2 - x$) of an AF culture harvested in the exponential growth phase recorded in 0.01 M NaCl, plotted against solution pH; error bars indicate the pH range over which the spectra were recorded.

titrations were not fully reversible). Furthermore, the ionic strength cannot be kept at 0.01 M at pH < 2. It is, however, possible to calculate the carboxyl speciation from the data, assuming that a certain percentage *f* of carboxyl groups is still deprotonated at the lowest experimental pH. In this case, eq 5 can be modified by introducing "*b*", representing the A_{COO^-} of residual deprotonated carboxyl groups at the lowest titration pH:

$$\frac{c_{COOH,\,x}}{c_{COO^-,\,x}} = \frac{\Delta A_{COO^-,10-x}}{-\Delta A_{COO^-,2-x} + b} \tag{9}$$

with

$$b = \frac{-f \times \Delta A_{COO^-,2-10}}{1 - f} \tag{10}$$

Figure 10B shows the resulting speciation if we assume that the model is correct and use the calculated residual deprotonation to correct the IR data using eqs 9 and 10. Even under this assumption, the titration data do not match the model predictions for 0.01 M ionic strength.

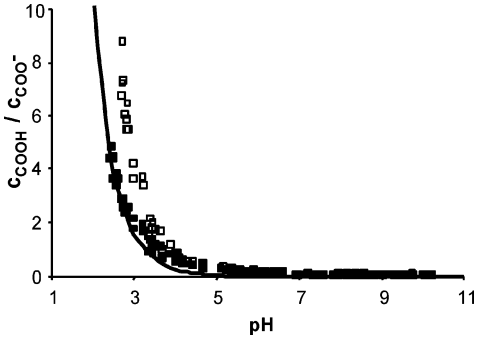

Figure 12. Carboxyl speciation for two exponential phase cultures of AF titrated at 0.5 M ionic strength (□) and adjusted for incomplete protonation according to the model (■) plotted against pH; the line represents speciation output for site 1 of the model at 0.5 M ionic strength.

In order to explore the influence of ionic strength on the carboxyl speciation, the same procedures as described above were applied to IR titrations conducted at an ionic strength of 0.5 mol L^{-1}. The results are shown in Figures 9B and 12. The data closely resemble those from 0.01 M ionic strength titrations shown in Figures 9A and 10, indicating no significant effect of ionic strength on the carboxyl speciation. The model prediction for carboxyl speciation at 0.5 M ionic strength, on the other hand, is quite different from that at 0.01 M. Interestingly, at an ionic strength of 0.5 M, the model shows much better agreement with the IR-generated data. This variation in the agreement between model and data with changing ionic strength suggests that the employed electrostatic model does not adequately describe the interactions occurring on the bacterial cell surface.

General Discussion

Batch acid−base titrations at 0.01 M ionic strength and electrophoretic mobility measurements at different pH values and ionic strengths were conducted on whole cells of AF. The program FITMOD was used to determine a two-site Donnan model, which was able to describe both data sets. Underlying the calculation of FITMOD models are chemical equilibrium reactions, which are meant to represent actual functionalities within the specimen. Spectroscopy is frequently cited as the tool of choice to test these models. In situ ATR-IR spectroscopy appears to be particularly suited for the task of detecting functional groups noninvasively.

The model suggests that there are two types of functional groups on the bacterial surface (Table 1). On the basis of the proposed deprotonation reactions and the calculated pK_a values, sites 1 and 2 represent carboxyl and amino groups, respectively, both of which are generally present in bacterial cell walls.

IR spectra confirmed the presence of carboxyl groups corresponding to site 1. Additionally, there was evidence for phosphodiester groups. A positively charged group corresponding to site 2 of the model was implicated by electrophoretic mobility data; however, IR data could not unequivocally confirm the presence of amino groups.

Following the identification of functional surface groups by spectroscopy, we also sought direct evidence of the deprotonation behavior of functional groups to compare with the calculated speciation of the model sites. Our focus in this respect had to be on carboxyl groups (site 1), as we were not able to monitor amino groups by IR.

Direct measurements of the pK_a values of bacterial surface groups are hampered by several practical restraints. When a

functional group is represented by sharp, well-separated peaks, pK_a determination is, in principle, straightforward as long as the Beer−Lambert law is obeyed and the total concentration (or absorbance) of the group can be measured. While the Beer−Lambert law is assumed to be applicable, in our investigations, the complete protonation and deprotonation required to assess the total carboxyl concentration via difference spectra could not be achieved, and therefore neither the total carboxyl concentration nor the molar absorption coefficient of the bacterial carboxyl groups could be determined experimentally. This meant that the IR data alone could not provide a pK_a value. Comparison of the IR data and the model predictions for carboxyl speciation at different ionic strengths suggests that the ability of the model to account for ionic strength and/or surface interactions is limited. The Donnan model assumes the even distribution of functional groups throughout a constant volume. Absorbance changes of the bacterial spectrum with pH as well as ionic strength have been attributed to the contraction/expansion of charged bacterial surface polymers such as extracellular polysaccharides.[27] Furthermore, bacterial cell walls themselves have been shown to contract/expand in response to pH and ionic strength changes.[56] In both cases, the assumption of a constant Donnan volume is not fulfilled for titration at 0.01 M ionic strength. Absorbance changes during titrations at 0.5 M ionic strength were much smaller. It is not clear if this is a factor in the better agreement obtained at this ionic strength. Better reproducibility between the replicate titrations at 0.5 M ionic strength further suggests that high ionic strength might be a more suitable system for IR studies than 0.01 M. The greater screening effect of electrolyte ions might also reduce electrostatic interactions on the surface, simplifying the interpretation of the results. While electrostatic interactions are accounted for by the Donnan model, other types of interactions are not included in the model, which may help explain why the calculated influence of ionic strength on carboxyl speciation does not agree with the IR data. Gershewitz et al. titrated self-assembled monolayers with carboxyl functional groups and found indications that surface carboxyl groups existed in free and differently hydrogen-bonded forms.[57] On bacterial surfaces, carboxyl groups may exist hydrogen bonded to each other as well as to other types of functional groups. Similarly, Sutheimer et al.[58] found in their titrations of polycarboxylic acids that polar, H-bonding, and steric effects as well as charge−charge interactions should be considered to account for ionic strength effects.

Additionally, IR data showed evidence of phosphodiester groups. The pK_a value of these groups could not be identified via IR; however, the data show that the pK_a lies below 4. The model only contains one site with a pK_a below 4, which, in agreement with the modeling literature, has been assigned to carboxyl groups. Considering the spectral data, it seems that site 1 more accurately encompasses carboxyl and phosphodiester contributions. In terms of the changes in charge ($0 \rightarrow -1$), the deprotonation reaction of a phosphodiester is the same as that of a carboxyl group. Furthermore, the two groups deprotonated within overlapping pH ranges. This may explain why one average site is able to describe batch acid−base titration data. Considering this, we cannot expect perfect agreement between IR carboxyl speciation and calculated speciation of site 1; however, it probably does not explain the differences in ionic strength response between the model and the data. While the model data do not contradict the IR spectral data, specific assignments should be made, if at all, with caution.

As previously mentioned, bacterial titration data are frequently modeled invoking a three-site model including a "phosphoryl" site deprotonating at a pH of 6−7. The proposed deprotonation reaction is of the form

$$R{-}PO_4H \rightleftarrows R{-}PO_4^- + H^+$$

that is, an uncharged functional group that acquires a single negative charge upon deprotonation.[3,10−12] It is unclear what actual structure in the bacterial cell wall this site could correspond to. The most common type of "phosphoryl" site in a gram-positive cell wall is a phosphodiester group. While the charge balance of the deprotonation reaction corresponds to this type of site, the pK_a for a phosphodiester is usually below 2 (and the presented spectral data roughly suggest a pK_a of <4 for phosphodiesters). There might also be phosphomonoester groups present on bacteria (e.g., in phosphorylated sugars or amino acids). The second pK_a of a phosphomonoester agrees with the "phosphoryl" site pK_a of 6−7; however, in the corresponding deprotonation reaction, a singly negatively charged group acquires a second negative charge ($-1 \rightarrow -2$). Although the proposed two-site model does not agree with many of the previously published modeling results for bacteria, it is supported by the spectral data. With other bacteria, particularly gram-negative cells, where the cell walls contain lipopolysaccharides, a significant contribution to the buffering capacity from phosphomonoesters in the mid pH range might be found.

In conclusion, while practical restraints make quantitative statements based on ATR-IR spectroscopy difficult, pH difference IR data allowed the identification of some functional groups on the cell wall and gave indications for pK_a values of carboxyl and phosphodiester groups. Positively charged surface groups, on the other hand, could not be identified. A two-site chemical equilibrium model using a Donnan electrostatic model was able to describe batch acid−base titration and electrophoretic mobility data. Comparison of the model with the IR data indicated that site 1 might, in fact, represent two chemically different sites. Changes in ionic strength affected model predictions much more than the IR spectral data. While it is desirable to describe the complex situation on the bacterial cell wall with the simplest model possible, care should be taken when relating proposed model sites to actual functionalities, and, in order to be able to accurately portray a wide range of experimental conditions, the electrostatic model might have to be revisited.

Acknowledgment. This research was funded by the New Zealand Foundation for Research, Science and Technology (Contract C05 X 0303: Extremophilic Microorganisms for Metal Sequestration from Aqueous Solutions). We thank Bruce Mountain, Marshall Muller, Moya Appleby, Ann Noddings and Chris Searle at GNS Taupo for assistance with acid−base titrations, Kevin Crump and the School of Pharmacy, University of Otago, for technical support of electrophoretic mobility measurements, Richard Easingwood and the Otago Centre for Electron Microscopy (OCEM) for assistance with electron microscopy, Brian Niven of the CASM Unit, University of Otago, for assistance with statistical analysis, and Cushla McGoverin and Keith Gordon for help with PCA.

LA062401J

(56) Ou, L. T.; Marquis, R. E. *J. Bacteriol.* **1970**, *101*, 92−101.
(57) Gershevitz, O.; Osnis, A.; Sukenik, C. N. *Isr. J. Chem.* **2005**, *45*, 321−336.
(58) Sutheimer, S. H.; Ferraco, M. J.; Cabaniss, S. E. *Anal. Chim. Acta* **1995**, *304*, 187−194.
(59) Krueger, R. G.; Gillham, N. W.; Coggin, J. H., Jr. *Introduction to Microbiology*; The Macmillan Company, Collier−Macmillan Publishers: London, New York, 1973.
(60) Schmidt, W. *Optical Spectroscopy in Chemistry and Life Sciences: An Introduction*; Wiley-VCH Verlag GmbH & Co.: Weinheim, Germany, 2005.
(61) Smith, B. C. *Quantitative Spectroscopy: Theory and Practice*; Academic Press: San Diego, CA, 2002.